Supplemental Material

Methods:

Nomenclature

We have employed the conventional and distinct rules of nomenclature for disease, lesion, human gene, and mouse gene. The human inherited disease Cerebral Cavernous Malformation, or the vascular lesion (in any species) that characterizes the phenotype, is abbreviated as CCM. The human *CCM3* gene is fully capitalized and italicized; the murine *Ccm3* gene is italicized with both upper- and lower-case letters.

Mouse Procedures

All animal procedures were approved by the Duke University Institutional Animal Care and Use Committee. The endothelial-specific, tamoxifen-inducible cre recombinase (*PDGFb-iCreERT2*)[13], lox-P flanked and knockout *Ccm3* alleles[14], and the Brainbow2.1, commonly referred to as confetti, reporter allele (*R26R-Confetti*)[15, 16] were bred into C57BL/6J mice with the following experimental genotype: *PDGFb-iCreERT2*, $Ccm3^{fl/KO}$, $R26R\text{-}Confetti^{fl/wt}$. The control C57BL/6J mice had the following control genotype: *PDGFb-iCreERT2*, $Ccm3^{wt/wt}$, $R26R\text{-}Confetti^{fl/wt}$. A single intragastric injection of 2µg of tamoxifen (Sigma T5648), dissolved in a 9:1 corn oil to ethanol solution, was administered to experimental mice on postnatal day (P) 3, 4, or 5 and on P3 for the control mice. The experimental mice injected on P3 were euthanized on P39 (female), P4 on P48 (female), and P5 on P53 (male). The control mouse injected on P3 was euthanized on P25 (female).

Brain Processing

Following CO_2 euthanasia, we performed cardiac perfusion with phosphate buffered saline (PBS) and 4% paraformaldehyde (PFA). The brains and eyes were carefully dissected in stored in 4% PFA overnight at 4C. Serial sectioning of the brains into 80-µm thick slices was performed with a vibrating microtome (Leica VT1000 S, Frequency: 8, Speed: 5). The slices were mounted onto slides with Fluoromount-G (SouthernBiotech 0100-01) for confocal microscopy. Low magnification images of brain slices were acquired with a stereo microscope under dark field illumination (Leica M165 FC).

Retina Immunofluorescence

Heat-induced antigen retrieval of the dissected retinas was performed with 10mM citric acid with 0.05% Tween20 (J.T. Baker X251-07) (pH 6) buffer for 5 minutes at 85C. Retinas were permeabilized with 1.0% triton X-100 (Sigma X100) blocked with 10% normal goat serum (Sigma G6767), incubated with rabbit anti-pMLC2 (1:200, Cell Signaling 3674S) overnight at 4C, incubated with Alexa Fluor 647 goat anti-rabbit IgG (Invitrogen A21244) for 2 hours at room temp, and mounted onto slices with Fluoromount-G (SouthernBiotech 0100-01) for confocal microscopy.

Confocal Microscopy

Images were acquired with a Zeiss 880 inverted confocal microscope equipped with GaAsP high QE 32 channel spectral array detector and 2 standard alkali PMTs for far-red detection. The brain slices were imaged with a 20x (0.80 NA) air objective. The retinas were imaged with the same 20x (0.8 NA) air objective and a 40x (1.2 NA) water objective. A Z-series for each brain region of interest was acquired through the full thickness of the sample with a step size of 2.5µm.

3D Image Reconstruction

Z-series from serial slices, each containing part of the CCM of interest, were aligned, utilizing white and gray matter boundaries, and concatenated in ImageJ. Uniform adjustments of brightness, contrast, and gamma for the concatenated images were performed with IMARIS 9.0. Each channel was assigned its respective confetti color for display. The surface tool of IMARIS was used to manually

outline the vascular lumens of the malformations to provide a visual aid in identifying the CCMs as well as to approximate the CCM volume. The dots tool of IMARIS was used to manually assign 3D coordinates (x,y,z) to the ECs within the experimental and control brain slices. The x,y,z positions of the ECs were exported for the nearest neighbor analysis.

Image Analysis

The nearest neighbor (NN) distances were calculated using the knn.dist function of the Fast Nearest Neighbor (FNN) 1.1 R package. The computer simulations were performed with a random number generator in R followed by the same NN algorithm applied to the experimental and control brain slice data. All graphs were prepared with Prism 7 software. Error bars on applicable graphs are shown as mean $\pm$ standard deviation.

Statistical Analysis

All statistical analysis was performed with IBM SPSS Statistics Version 25. We tested the assumption of equal variance in our CCM and control NN distance data sets with Levene's test. With the exception of the 2nd NN pair for the CFP CCM and control data sets (Fig 3D), all data sets rejected the null hypothesis of equal variance; therefore, we used the Mann-Whitney test to compare CCM and control NN distances. Comparisons were considered statistically significant when p-value < 0.05.

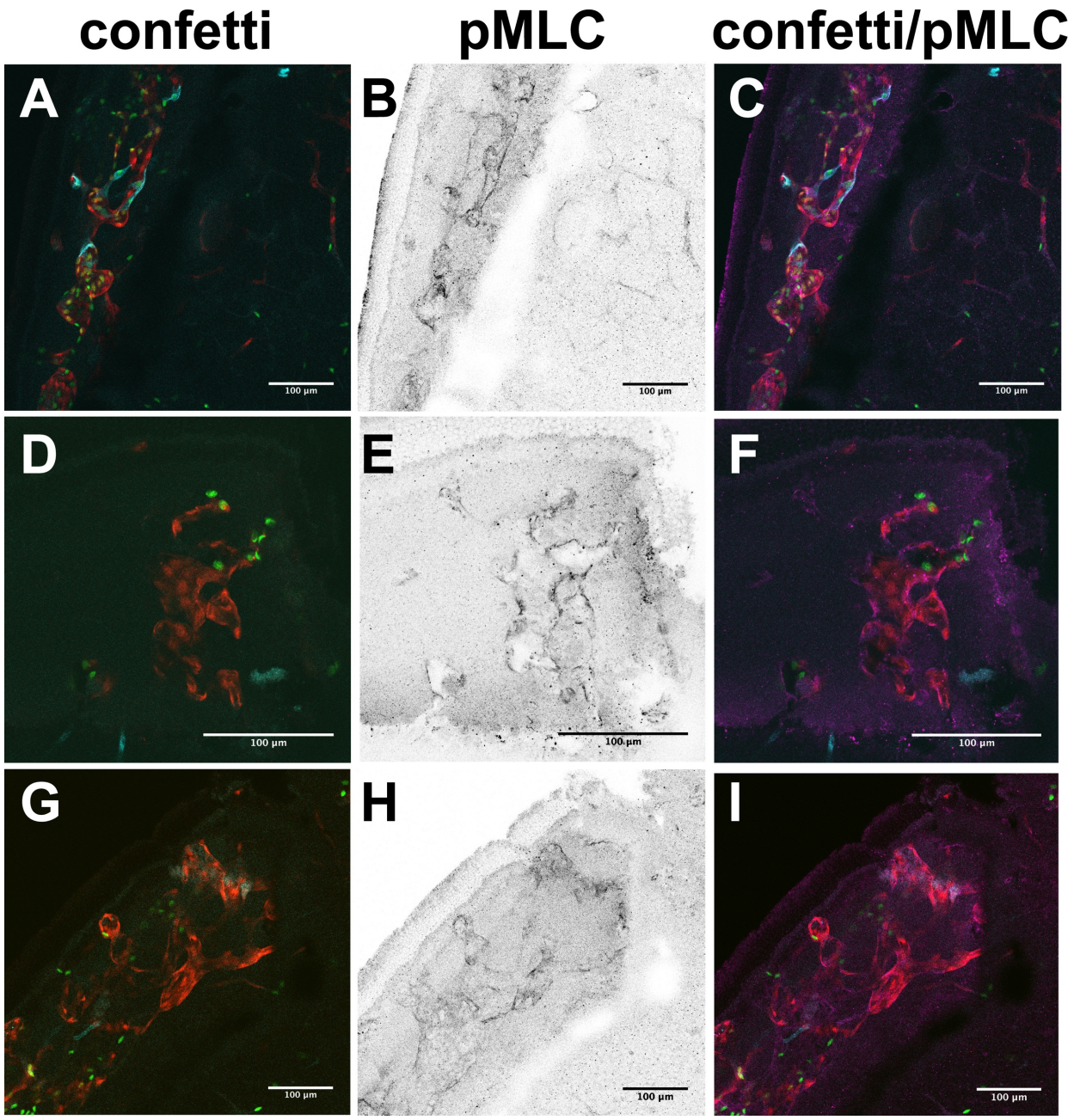

Online Figure I. Transient cre recombinase activity deletes the *Ccm3* allele and recombines the *R26R-Confetti* allele within individual ECs that line CCMs. The developing vasculature at the periphery of the retina becomes malformed in this CCM mouse model and provides a tractable tissue to perform whole mount antibody staining. To increase the malformation burden, these mice (*Ccm3*$^{fl/KO}$, *PDGFb-iCreERT2*, *R26R-Confetti*$^{fl/wt}$) were injected with 25µg of tamoxifen. Phospho-myosin light chain (pMLC) is upregulated in Ccm-null cells and was used as a secondary marker for *Ccm3* deletion.[1,2] The colocalization of a confetti color and the increase in pMLC signal identifies an individual EC in which the *Ccm3* and *R26R-Confetti* alleles have undergone cre recombination. The confetti colors, pMLC staining with Alexa Fluor 647, and the composite image are shown for three regions of CCMs (A-C, D-F, G-I). No YFP labeled ECs were detected in these regions. The lack of signal is likely due to YFP denaturation during the heat-induced antigen retrieval necessary for the pMLC staining. The ECs within these

malformations that are labeled with a confetti color also have an increase in pMLC staining. Thus, both recombination events (deletion of the *Ccm3* allele and labeling with a confetti color) are able to occur within the same EC of this mouse model.

Online Video I. 3D reconstruction of 6 serial brain slices containing a large, multicavernous CCM composed of clonally dominant ECs labeled with YFP. Gray translucent surfaces have been added to this 3D reconstruction to aid in visualizing the CCM lumens. This sample also contains a second CCM, located in the lower left-hand region, composed of clonally dominant ECs labeled with nGFP. All four confetti colors are visualized throughout this sample. The ability to detect each confetti color reduces the probability that an unlabeled EC (appearing as a blank region of the CCM) has undergone cre recombination as we are able to detect all ECs which have recombined at the confetti locus. The background level of confetti labeling in the brain regions that are not part of the CCM also demonstrate the low rate of cre recombination we induced with the single, 2-μg dose of tamoxifen.

Online Video II. 3D reconstruction of 2 serial brain slices containing a large, single-cavern CCM composed of clonally dominant ECs labeled with nGFP. Gray translucent surfaces have been added to this 3D reconstruction to aid in visualizing the CCM lumens. This sample also contains other CCMs, located in the upper region, composed of clonally dominant ECs labeled with RFP.

Online Video III. 3D reconstruction of 4 serial brain slices containing a small CCM composed of clonally dominant ECs labeled with mCFP. Gray translucent surfaces have been added to this 3D reconstruction to aid in visualizing the CCM lumens.

Online Video IV. 3D reconstruction of 4 serial brain slices containing multiple small, single-cavern and multicavernous CCMs composed of clonally dominant ECs labeled with RFP. Gray translucent surfaces have been added to this 3D reconstruction to aid in visualizing the CCM lumens.

Online Video V. Visual representation of the NN distances for 2 nGFP ECs within a large CCM composed of clonally dominant ECs labeled with nGFP. The first rotation is the 3D reconstruction of the CCM used for the sample NN analysis described in Figure 2. The second rotation visually depicts the distances from one EC to all of the other ECs within the CCM. The third rotation visually depicts the distances from a different EC to all of the other ECs within the CCM. While not shown in the video, the NN algorithm continues until the distances between every EC within the CCM have been calculated and ranked from smallest to largest. The complete set of NN distances are shown in Figure 2G.

Online Video VI. Visual representation of the NN distances for 2 nGFP ECs within the non-lesion control brain slices. The first rotation is the 3D reconstruction of the control brain slices used for the sample NN analysis described in Figure 2. The second rotation visually depicts the distances from one nGFP-labeled EC to all of the other nGFP-labeled ECs within the sample. The third rotation visually depicts the distances from a different nGFP-labeled EC to all of the other nGFP-labeled ECs within the sample. While not shown in the video, the NN algorithm continues until the distances between every nGFP-labeled EC within the control brain sample have been calculated and ranked from smallest to largest. The complete set of NN distances are shown in Figure 2G.

Online Video VII. 3D reconstruction of a small, multicavernous CCM composed of clonally dominant ECs labeled with RFP. Gray translucent surfaces have been added to this 3D reconstruction to aid in visualizing the CCM lumens. This 3D reconstruction contains the CCM shown in Fig 4A.

Online Video VIII. 3D reconstruction of a large, multicavernous CCM composed of clonally dominant ECs labeled with YFP along with unlabeled, wild type ECs. Gray translucent surfaces have been added to this 3D reconstruction to aid in visualizing the CCM lumens. This 3D reconstruction

contains the CCM shown in Fig 4B as well as a second CCM containing clonally dominant ECs labeled with nGFP.

References:

1. Stockton RA, Shenkar R, Awad IA and Ginsberg MH. Cerebral cavernous malformations proteins inhibit Rho kinaseto stabilize vascular integrity. *The Journal of experimental medicine*. 2010;207:881-96.
2. Borikova AL, Dibble CF, Sciaky N, Welch CM, Abell AN, Bencharit S and Johnson GL. Rho kinase inhibition rescues the endothelial cell cerebral cavernous malformation phenotype. *The Journal of biological chemistry*. 2010;285:11760-4.